REPORT

ROBOTICS

A tailless aerial robotic flapper reveals that flies use torque coupling in rapid banked turns

Matěj Karásek[1]*, Florian T. Muijres[2], Christophe De Wagter[1], Bart D. W. Remes[1], Guido C. H. E. de Croon[1]

Insects are among the most agile natural flyers. Hypotheses on their flight control cannot always be validated by experiments with animals or tethered robots. To this end, we developed a programmable and agile autonomous free-flying robot controlled through bio-inspired motion changes of its flapping wings. Despite being 55 times the size of a fruit fly, the robot can accurately mimic the rapid escape maneuvers of flies, including a correcting yaw rotation toward the escape heading. Because the robot's yaw control was turned off, we showed that these yaw rotations result from passive, translation-induced aerodynamic coupling between the yaw torque and the roll and pitch torques produced throughout the maneuver. The robot enables new methods for studying animal flight, and its flight characteristics allow for real-world flight missions.

Flying insects demonstrate extraordinary agility when they reject wind gusts (*1*), catch prey (*2*), or evade a human hand trying to swat them (*3*). Such aerobatic feats, enabled by unsteady aerodynamics (*4*, *5*), require both quick and precise reactions of their neural sensory-motoric control system (*6*). Research into the underlying mechanisms typically involves in vivo observations of flight maneuvers, usually via high-speed cameras, and has yielded hypotheses on possible control strategies during maneuvers such as saccades (*7*), evasive maneuvers (*3*), or aerial tumble recovery (*8*). These hypotheses are currently being tested using theoretical modeling (*8*) or tethered, dynamically scaled robots (*9*). However, such tests are incomplete; existing theoretical models lack sufficient fidelity, and tethered robots cannot model the full movement dynamics experienced during free flight.

Lately, many bio-inspired robotic platforms have been developed that try to mimic the flapping flight of hummingbirds (*10*, *11*), bats (*12*), beetles (*13*), and even flies (*14*). Unlike traditional fixed-wing and rotary-wing robots, which differ greatly from flying animals and thus experience different flight dynamics, flapping-wing vehicles could be used to test existing hypotheses on animal flight control through systematic and programmable experiments with known internal processes (*15*, *16*). Nonetheless, because of technological challenges arising from stringent weight and size restrictions, most existing designs cannot match the flight performance of their biological counterparts; they lack the necessary agility, sufficient power to take off, or sufficient energy to fly for more than a minute. The state-of-the-art Nano Hummingbird (*10*) and Robobee (*14*) come close in terms of performance and autonomous flight control, respectively. However, the Nano Hummingbird must be manually operated by a trained human pilot and thus cannot fly autonomously (*10*), whereas the fly-sized Robobee is tethered to an off-board power supply, which limits its maneuvering capabilities (*14*).

Here, we present a fully programmable autonomous and freely flying insect-inspired robot that is agile both around hover and in fast forward flight (Fig. 1). The robot is tailless, and thus, as in flies (*5*, *8*), position and orientation in space are controlled solely through wing motion adjustments. When designing the robot, we built upon the reliable flapping mechanisms with flexible wings found in (*17*). Two wings on each side of the robot flap in counterphase and clap and peel with each other to enhance the produced thrust (movie S1), inspired by the clap-and-fling mechanism observed in nature during thrust-demanding tasks (*4*). The size, wing morphology, and wing kinematics of our robot do not mimic any specific natural flyer but were instead optimized for maximal power efficiency when driven by miniature brushless DC motors, an engineering alternative to the powerful animal flight muscles. The resulting 28.2-g robot has a wingspan of 33 cm (Fig. 1A); its 14-cm-long wings have a flapping frequency of approximately 17 Hz in hover. The power efficiency of our robot enables a flight endurance of 5 min in hover, or a flight range of more than 1 km, on a single battery charge. These performance characteristics allow for a wide variety of (automated) experiments and even real-world missions.

To control its orientation, the robot produces torques around the three orthogonal body axes via bio-inspired adjustments of the wingbeat pattern (Fig. 1, H to J). As in fruit flies (*5*, *8*), yaw torque is produced by changing the wing root angle such that the (wingbeat-average) thrust vectors of the left and right wing(s) are tilted in opposite directions (Fig. 1, E and H). Pitch torques are generated by adjusting the dihedral angle (center line of the flapping wings), which, as in fruit flies (*5*), shifts the wing thrust vectors relative to the center of mass (CoM) (Fig. 1, F and I). Roll torques are produced by generating a thrust difference between the left and right wing (pair). Flies have a coupled wingbeat actuation system and achieve this using asymmetric stroke amplitude adjustments (*5*), whereas our robot adjusts stroke frequencies (Fig. 1, G and J). Finally, symmetric flapping frequency variation is used for modulation of thrust magnitude. The resulting control torques and thrust have high magnitude (figs. S1 and S2), high bandwidth (fig. S3), and very little coupling (figs. S3 to S5) and are minimally sensitive to the vertical location of the CoM (fig. S5, E and F) (*18*).

Tailless flapping flight is unstable near hover (*19*), and thus the robot needs to actively stabilize its attitude (orientation in space). To this end, it carries a miniature 2.8-g autopilot (*20*) equipped with a programmable microcomputer and sensors for attitude estimation (*18*)—that is, a three-axis gyroscope and accelerometer (fig. S6). Attitude control (fig. S7) uses the estimated attitude as well as the body rotation rate signals from the gyroscopes (*18*) and is in many respects comparable to the haltere-based proportional-integral (PI) controller suggested to be used by fruit flies (*5*, *8*). Apart from remotely piloted operation, the autopilot allows execution of preprogrammed control sequences triggered by the pilot.

Similar to many flying insects (*3*, *5*), the robot can actively control four degrees of freedom (DOFs): roll, pitch, yaw, and thrust. To enable movement in a six-DOF space, translation control follows the helicopter model, whereby forward/backward flight speed is controlled via body pitch (Fig. 1C and movie S2) and sideways flight is achieved by rolling the body left or right (Fig. 1D and movie S3). The robot can perform stationary hovering flight and move in any direction with rapid, yet smooth and reproducible transitions (figs. S9 to S12 and movie S4). In forward flight, the highest power efficiency is achieved around 3 m/s; applying full power results in the maximal speed of 7 m/s. The maximal sideways speed is 4 m/s.

The key property of interest here is the robot's agility, which is exceptional for a flapping-wing robot and approaches that of rotorcraft robots (*21*). It can perform 360° roll and pitch flips, during which it reaches angular accelerations of up to about 5000° s^{-2} (figs. S13 and S14 and movies S5 and S6). Its maximal thrust-to-weight ratio of 1.3 allows for quick climbs, although it remains inferior to the best natural fliers with thrust-to-weight ratios of ≥2 (*3*).

[1]Micro Air Vehicle Laboratory, Control and Simulation, Delft University of Technology, Delft, Netherlands. [2]Experimental Zoology Group, Wageningen University and Research, Wageningen, Netherlands.
*Corresponding author. Email: m.karasek@tudelft.nl

Despite the large variation in size, mass, wing kinematics, and wing morphology among flapping-wing fliers, they all experience the same type of passive aerodynamic damping, termed flapping countertorque and flapping counterforce (*22*), and thus their flight dynamics share similar characteristics (*19*). We can thus use the robot to study maneuver dynamics and control in a wide range of flying animals, from hummingbirds to tiny two-winged fruit flies. To demonstrate this potential for animal flight research, we programmed the robot to mimic the rapid banked turns observed in fruit flies when evading predators (movie S7) (*3*).

It has been hypothesized that these evasive maneuvers consist of two distinct phases (*3*, *5*). The first phase is simply a feedforward program triggered by the visually detected threat, whereby the fly produces a combined roll and pitch rotation, with the ratio of pitch rate to roll rate (q/p) defining the turn angle. The second recovery phase is controlled using sensory feedback provided by the halteres. It has also been hypothesized that fruit flies do not control body yaw throughout the evasive maneuver, but instead control for the sideslip caused by the maneuver after the turn, possibly by using much slower visual feedback (*3*, *5*, *9*).

We tested these two hypotheses by reproducing a range of evasive maneuvers described in fruit flies. These maneuvers were preprogrammed and fully autonomous to ensure that the control inputs were always the same. The initial phase of a maneuver was controlled using an open-loop combination of pitch and roll torque commands (*18*). For the recovery phase, we used feedback control of roll and pitch, whereas yaw control was turned off.

In our first set of experiments, we performed two evasive maneuvers initiated with different q/p values (measured at the end of the open-loop phase), the first dominated by rolling (q/p = 0.52; Fig. 2A and fig. S15), and the second dominated by pitching (q/p = 1.67; Fig. 2C and fig. S16). Despite substantial differences between our four-winged robot and the much smaller two-winged fruit fly, the robotic maneuvers resembled those observed in fruit flies remarkably well (Fig. 2, A to D, and movies S8 and S9). To enable quantitative comparison of the fruit fly and robot maneuvers, we normalized distances by wing length and time according to wingbeat-cycle period (flies) and half-wingbeat-cycle period (robot) (figs. S17 and S18) (*18*) and determined the Pearson correlation coefficient c_r and normalized root mean square error (RMSE) between the normalized robot and fruit fly data (table S5). For both maneuvers (Fig. 2, A to D), we found high correlations and low RMSE (table S5), further highlighting the similarity.

Detailed analysis of a 90° turn initiated with 94% of the maximal pitch torque and 74% of the maximal roll torque (q/p = 0.54) (Fig. 2, E to I, fig. S19, and movie S10) shows that at the apex of the turn, an extreme body attitude of ~100° in roll is reached, which is comparable to the equivalent attitudes observed in fruit flies (Fig. 2B) (*3*). In

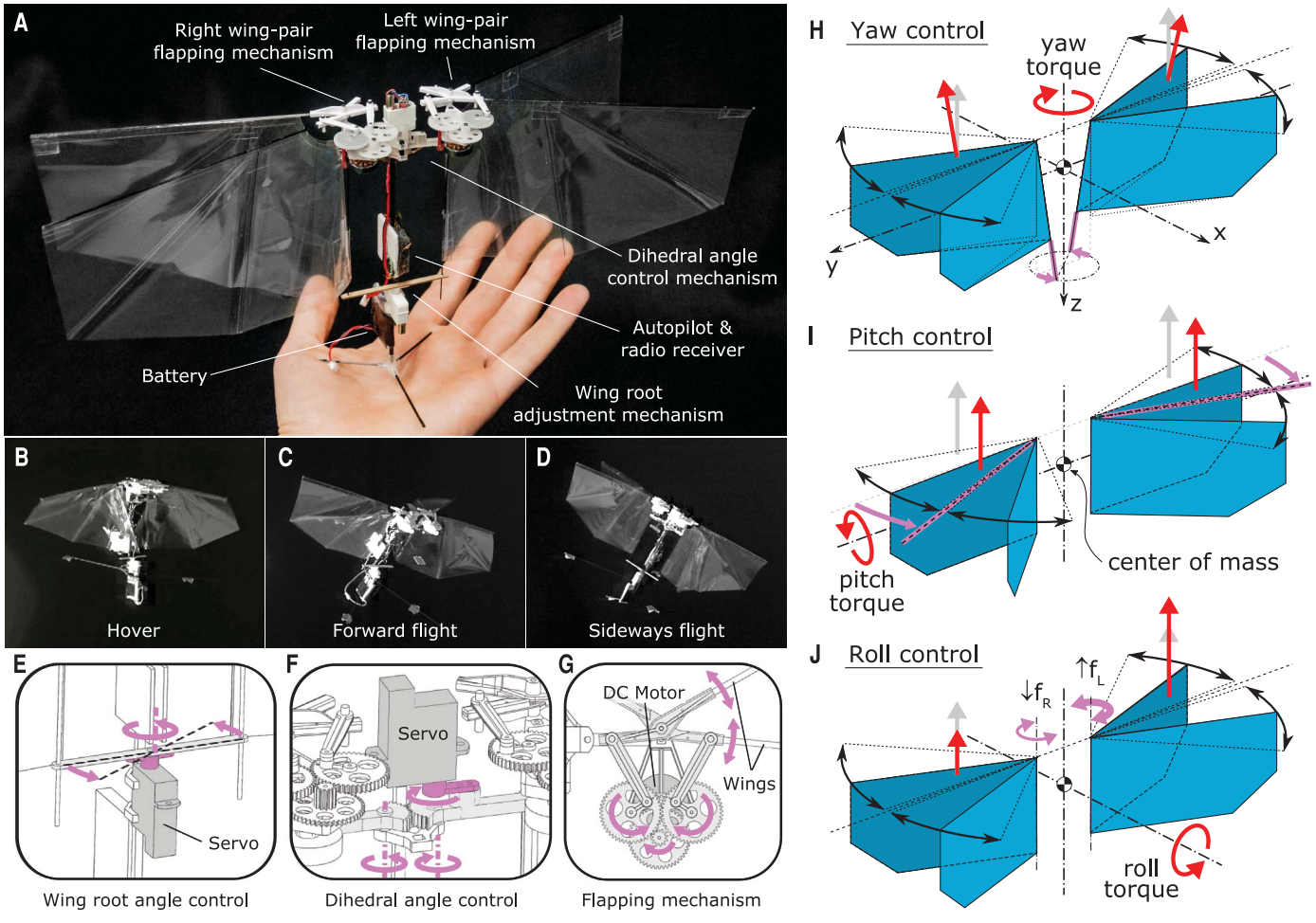

Fig. 1. An insect-inspired free-flying robotic platform is controlled through its two pairs of independently flapping wings. (**A**) Description of the robot's components. (**B** to **D**) High-speed camera frames capturing the robot in hover (B), forward flight (C), and sideways flight (D), from movies S1 to S3, respectively. (**E** to **G**) Details of the robot design: (E) the wing root adjustment mechanism for yaw torque control, (F) the dihedral control mechanism for pitch torque control, and (G) the flapping mechanism (of the left wing pair), used for thrust and roll torque control. (**H** to **J**) Wing actuation and aerodynamic forces and torques during yaw control (H), pitch control (I), and roll control (J). Magenta arrows show actuation action, gray arrows show the nominal wingbeat-average aerodynamic thrust vectors, and red arrows show wingbeat-average thrust and torques after control actuation.

the subsequent feedback phase, the transition between the positive and negative acceleration peaks (difference of 9000° s^{-2}) took fewer than three wingbeats (~0.18 s) while closely following the wing actuation that generates the body-accelerating torques (Fig. 2, G to I).

These results confirm that a rapid banked turn can be successfully achieved with an open-loop maneuver initiation and closed-loop recovery. Hence, they support the hypothesis that the recovery phase of the evasive maneuver in fruit flies is also controlled using a PI-like roll and pitch control system, whereby halteres might provide the sensory input (*3*, *5*).

To systematically test the relation between q/p and turn angle, we performed evasive maneuvers at five combinations of roll and pitch torque commands, varying q/p from ~0.3 to ~2.1 (Fig. 3 and figs. S20 and S21) (*18*). As shown in Fig. 3A, q/p had a clear effect on the flight trajectory, and in agreement with fruit flies, q/p was positively correlated with turn angle (c_r = 0.95; Fig. 3F), whereby turns with dominant pitch rates resulted in larger turn angles.

In agreement with the fruit fly experiments (*3*), we also observed high yaw rates in the direction of the turn during the recovery phase (Fig. 3D). Because no yaw command was provided during the robot maneuvers, these yaw movements were thus passively induced (Fig. 1).

For the robot as well as the fruit flies, the observed yaw accelerations $\dot{r}$ correlated strongly with the roll accelerations $\dot{p}$ and, particularly for

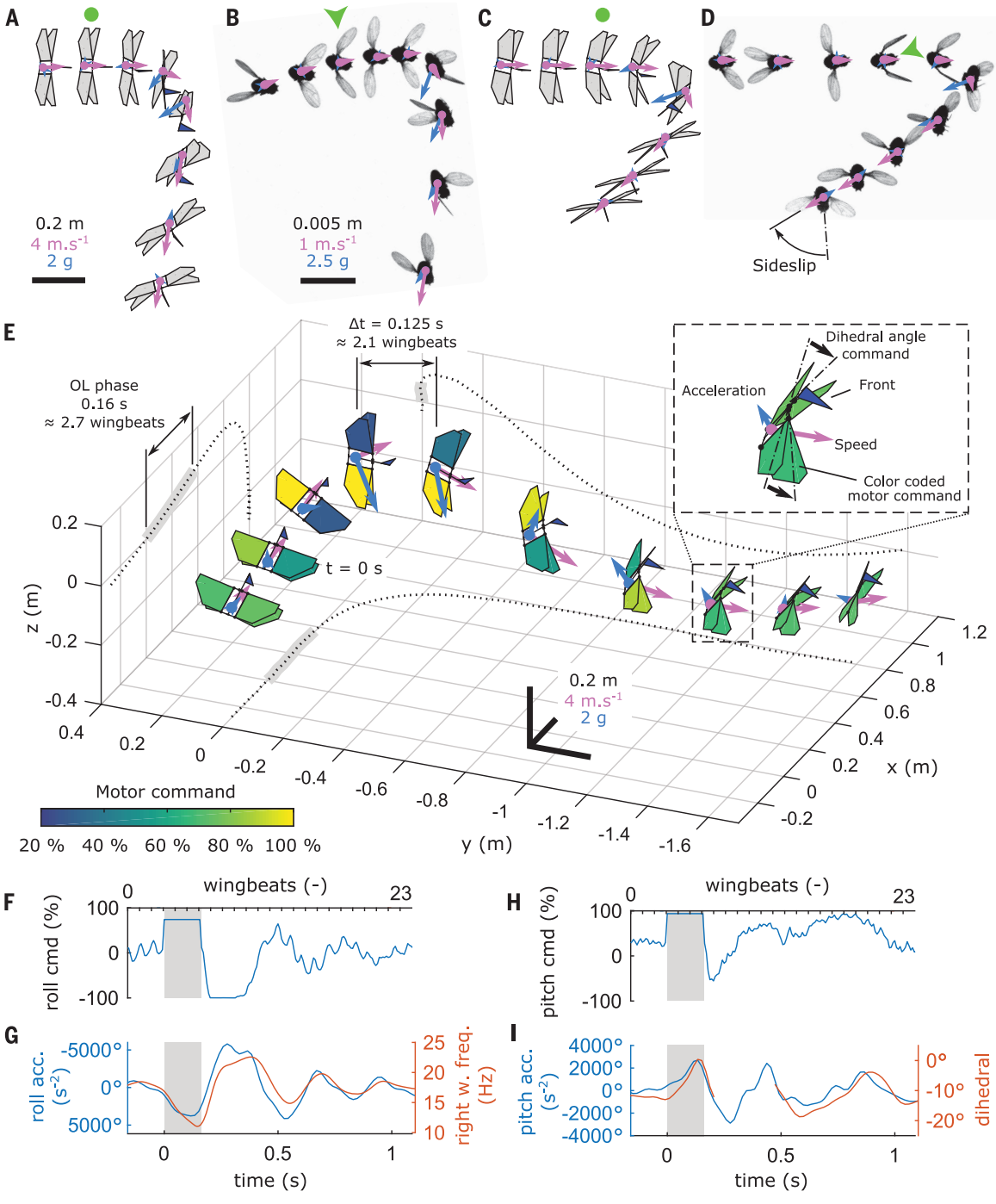

Fig. 2. The robot mimics rapid banked turns observed in escaping fruit flies. (**A** and **C**) Time sequences (top view) of a roll-dominated maneuver (pitch rate/roll rate ratio q/p = 0.52) and a pitch-dominated maneuver (q/p = 1.67), respectively. The start of the open-loop (OL) phase is marked with a green circle. (**B** and **D**) Time sequences (top view) of the equivalent fruit fly evasive maneuvers with the stimulus (green arrowhead) coming from the left and the front, respectively. (**E** to **I**) Detailed analysis of a roll-dominated maneuver (q/p = 0.54). (E) Time sequence with constant time interval of 0.125 s; trajectory projections are shown by dotted lines. Wings are color-coded according to thrust command magnitude, as shown in the color bar. [(F) to (I)] Time histories of roll command (F), roll acceleration and flapping frequency of the right wing pair (G), pitch command (H), and pitch acceleration and dihedral angle (I). In (A) to (E), blue and magenta arrows represent velocity and acceleration vectors, respectively; vectors (arrow lengths) are relative to the black scale bars in (A) and (E) for the robot and in (B) for flies. The OL phase in (F) to (I) is highlighted by gray background.

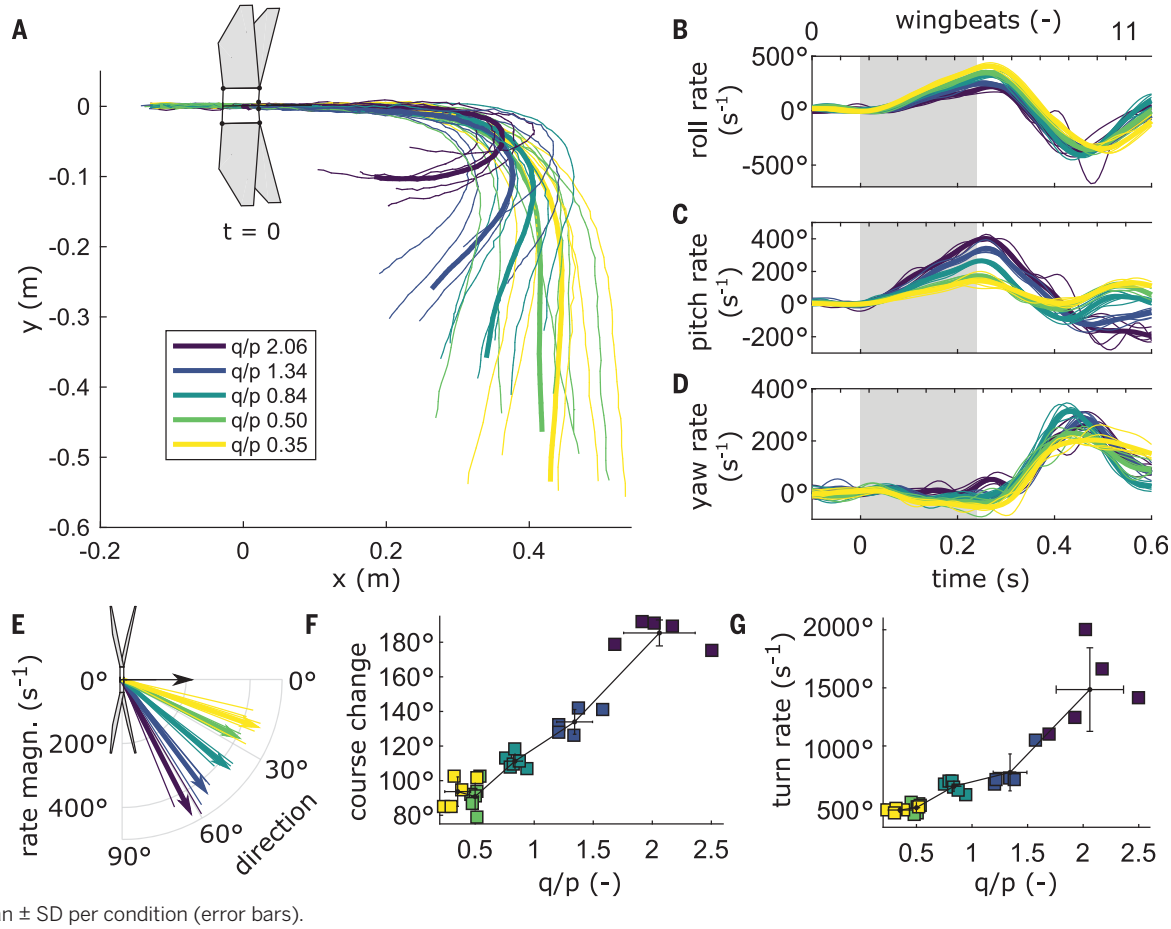

Fig. 3. The turn angle during the banked turn can be controlled by varying the ratio of pitch to roll torque commands. Results are color-coded [see key in (A)] according to the *q*/*p* ratio of the maneuver; thin lines are individual trials and thick lines are series averages. (**A**) Top view of trajectories, aligned at the start of the OL phase (t = 0 s) where the robot is shown. (**B** to **D**) Time histories of angular rates during the maneuvers. The OL phase is highlighted by gray background. (**E**) Angular rate vector in the horizontal body plane, relative to the forward-directed black arrow. (**F** and **G**) Turn angle and turn rate versus *q*/*p*, respectively, for individual tests (squares) and mean ± SD per condition (error bars).

the sharper turns (high *q*/*p*), also with the pitch accelerations $\dot{q}$ (Fig. 4, A and B). Moreover, the largest yaw accelerations were observed in the recovery phase, where both the robot and the flies move at relatively high forward and sideways flight velocities (fig. S22).

On the basis of these observations, and thanks to the simple wing kinematics of the robot (where roll torque and pitch torque are each modulated by only one parameter), we were able to develop a functional aerodynamic yaw torque model that explains the observed yaw accelerations in the robot maneuvers (Fig. 4, D to H, and fig. S23) (*18*):

$$N = \frac{\dot{r}}{I_{zz}} = -b\Phi R[(f_L + f_R)Rr + (f_L - f_R)u + (f_L + f_R)\Gamma v] \quad (1)$$

where N is yaw torque; $\dot{r}$ is yaw acceleration; I_{zz} is the moment of inertia around the vertical body axis; b is the linear damping coefficient due to flapping counterforce (*22*); Φ is flapping amplitude; R is wing length; f_L and f_R are flapping frequency of the left and the right wing, respectively; r is yaw rate; u and v are the forward and sideways velocity of the robot, respectively; and Γ is the wing dihedral angle.

The first term, $-b\Phi R(f_L + f_R)Rr$, represents the flapping countertorque (N_{FCT}), which is by definition opposite to the direction of yaw rate (Fig. 4F) (*22*) and thus cannot explain the observed yaw accelerations. The two remaining terms are our addition to the passive yaw-torque system for flapping flight, which we call translation-induced coupled yaw torque (N_{TCT}), as it models the coupling effect of roll and pitch torque production on yaw torque in the presence of translating body motions ($N_{TCT} = N_{u\&roll} + N_{v\&pitch}$; Fig. 4, G and H). Thus, in the presence of a forward velocity u, the differential flapping frequency ($f_L - f_R$) used for roll torque production also results in a yaw torque ($N_{u\&roll}$; Fig. 4G). Similarly, in the presence of a sideways velocity v, the dihedral angle Γ used for pitch torque production equally generates a yaw torque ($N_{v\&pitch}$; Fig. 4H). In steady hover conditions, such coupling is negligible (fig. S4).

Despite its low complexity, this model accurately estimates the observed yaw acceleration in both roll-dominated and pitch-dominated banked turn maneuvers [Fig. 4, D and E; c_r = 0.73 ± 0.30 (mean ± SD) for the five sets of trials in fig. S24 and table S6]. Notably, the model predicts the same coupling effects when differential flapping amplitudes are used for roll torque production (eqs. S10 to S14 and fig. S23), which is what many biological fliers as well as other aerial robotic flappers use.

Because fruit fly wing motion patterns are highly complex, we were unable to adapt the model for fruit flies, where multiple degrees of freedom are involved in generating roll and pitch torques. For the fruit fly maneuvers, we estimated yaw accelerations resulting from translation-induced coupled yaw torque as the measured acceleration minus the accelerations caused by flapping countertorque (eq. S19). Relative to our initial yaw-pitch and yaw-roll correlations (Fig. 4B), these flapping countertorque–corrected yaw accelerations $\dot{r}_{TCT}$ correlate even better with the product of roll acceleration and forward velocity, as well as with the product of pitch acceleration and sideways velocity (Fig. 4C); these findings suggest that translation-induced coupled yaw torque is also present in the fruit fly maneuvers.

Together with the high similarity between the turn dynamics of the robot and of the fruit flies (fig. S22), these results provide strong support for the hypothesis that fruit flies do not actively control yaw throughout evasive maneuvers (*3*, *5*), but instead use the translation-induced coupled yaw torque (Eq. 1) to rotate their body in the direction of the banked turn. Given that many maneuvers of flying animals occur at nonzero translational velocities (*2*–*4*, *7*, *22*–*24*), the passive

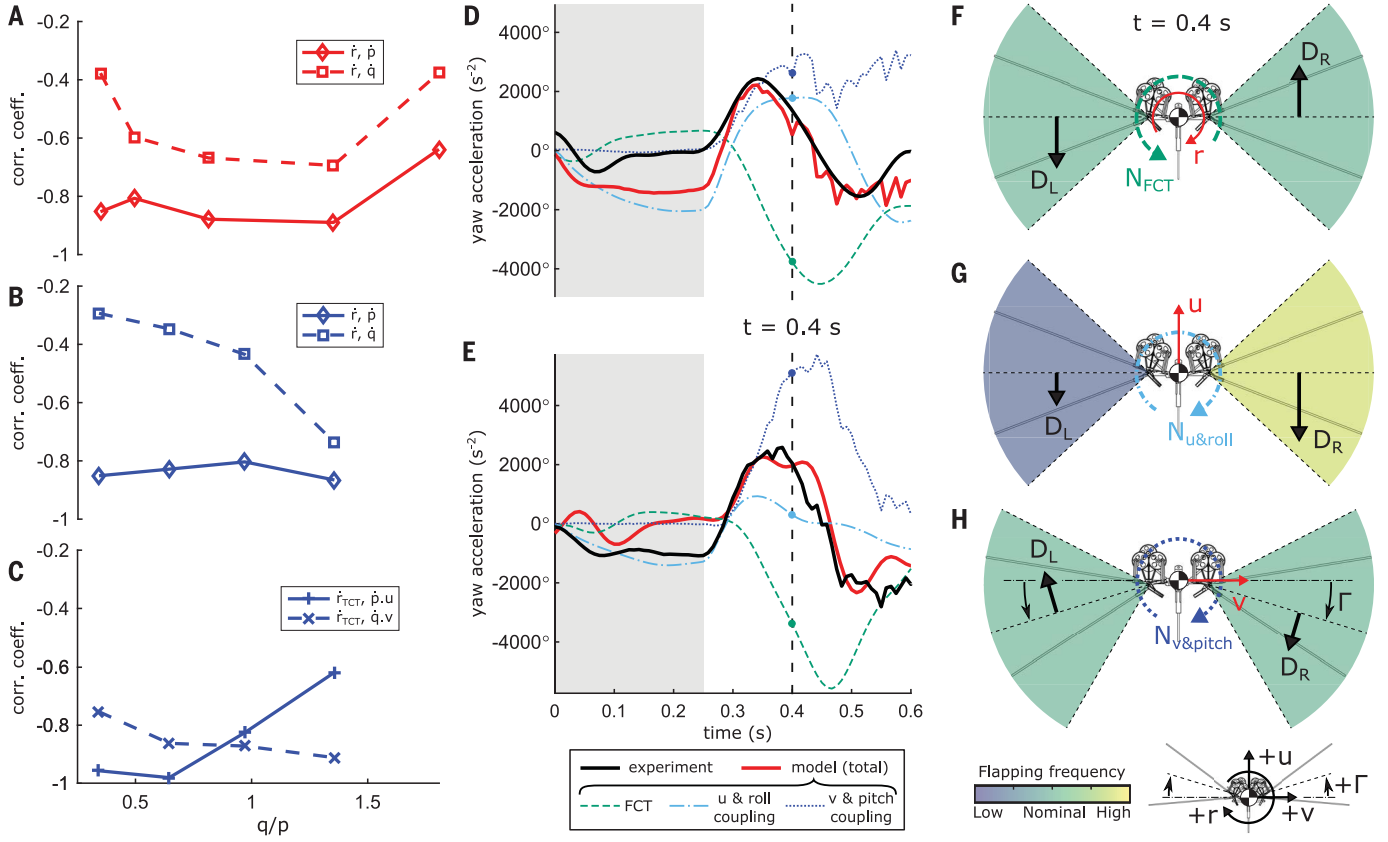

Fig. 4. The passive yaw accelerations during the recovery phase of banked turns originate from the coupling between the roll and pitch torque generation mechanisms and translational body motions. (**A** and **B**) Correlation coefficient between the yaw acceleration and the roll (solid) and pitch (dashed) accelerations at various pitch-to-roll rate ratios q/p for rapid banked turns produced by the robot (A) and for evasive maneuvers produced by fruit flies (B). (**C**) Correlation coefficients for the same evasive maneuvers of fruit flies, after correcting for the flapping countertorque and including the translational body velocities. (**D** and **E**) Measured (black) and modeled (red) yaw accelerations during the banked turn of the robot: (D) roll-dominated banked turn (q/p = 0.50), (E) pitch-dominated banked turn (q/p = 1.34). Line style of individual model components follows the legend below (E). (**F** to **H**) The three passive yaw torque–producing mechanisms at t = 0.4 s in (D) and (E) are flapping countertorque (F), torque due to forward motion with uneven left and right flapping frequencies (G), and torque due to sideways motion with nonzero dihedral angle (H). Color coding of the flapping frequency and the positive directions of all the coordinates are shown below (H). D_L and D_R are the wingbeat-average drag forces of the left and right wing pair, respectively, as defined by eq. S9.

torque coupling we have identified might be more widespread among natural flyers.

Despite the observed yaw accelerations, high sideslips remained at the end of the turns for both the robot and the flies (Fig. 2, A to D, and figs. S17, S18, and S22). In a separate set of robot experiments, we were able to completely remove this sideslip by producing feedforward maximum yaw torque throughout the recovery phase, but this body alignment did not increase the speed of the turn (figs. S25 and S26). Hence, producing such precisely timed and thus complex feedforward yaw command throughout the turn might not enable flies to increase evasive performance. This might be one of the reasons why flies prefer to rely on passive alignment throughout the turn and fully align their body actively only after the turn, possibly using a simpler feedback controller based on visual information (*3*, *5*).

REFERENCES AND NOTES

1. J. T. Vance, I. Faruque, J. S. Humbert, *Bioinspir. Biomim.* **8**, 016004 (2013).
2. S. A. Combes, D. E. Rundle, J. M. Iwasaki, J. D. Crall, *J. Exp. Biol.* **215**, 903–913 (2012).
3. F. T. Muijres, M. J. Elzinga, J. M. Melis, M. H. Dickinson, *Science* **344**, 172–177 (2014).
4. D. D. Chin, D. Lentink, *J. Exp. Biol.* **219**, 920–932 (2016).
5. M. H. Dickinson, F. T. Muijres, *Philos. Trans. R. Soc. B* **371**, 20150388 (2016).
6. W. Shyy, C. K. Kang, P. Chirarattananon, S. Ravi, H. Liu, *Proc. R. Soc. A* **472**, 20150712 (2016).
7. F. T. Muijres, M. J. Elzinga, N. A. Iwasaki, M. H. Dickinson, *J. Exp. Biol.* **218**, 864–875 (2015).
8. L. Ristroph *et al.*, in *Natural Locomotion in Fluids and on Surfaces*, S. Childress, A. Hosoi, W. W. Schultz, J. Wang, Eds. (Springer, 2012), pp. 83–99.
9. M. J. Elzinga, W. B. Dickson, M. H. Dickinson, *J. R. Soc. Interface* **9**, 1685–1696 (2012).
10. M. Keennon, K. Klingebiel, H. Won, A. Andriukov, "Development of the Nano Hummingbird: A Tailless Flapping Wing Micro Air Vehicle." Paper presented at the 50th AIAA Aerospace Sciences Meeting including the New Horizons Forum and Aerospace Exposition (2012).
11. A. Roshanbin, H. Altartouri, M. Karásek, A. Preumont, *Int. J. Micro Air Veh.* **9**, 270–282 (2017).
12. A. Ramezani, S.-J. Chung, S. Hutchinson, *Sci. Robot.* **2**, eaal2505 (2017).
13. H. V. Phan, T. Kang, H. C. Park, *Bioinspir. Biomim.* **12**, 36006 (2017).
14. K. Y. Ma, P. Chirarattananon, S. B. Fuller, R. J. Wood, *Science* **340**, 603–607 (2013).
15. N. Franceschini, F. Ruffier, J. Serres, *Curr. Biol.* **17**, 329–335 (2007).
16. M. Kovač, *Soft Robot.* **1**, 28–37 (2014).
17. G. C. H. E. de Croon, M. Percin, B. D. W. Remes, R. Ruijsink, C. De Wagter, *The DelFly—Design, Aerodynamics, and Artificial Intelligence of a Flapping Wing Robot* (Springer, 2016).
18. See supplementary materials.
19. M. Sun, J. Wang, Y. Xiong, *Lixue Xuebao* **23**, 231–246 (2007).
20. B. D. W. Remes *et al.*, in *IMAV 2014: International Micro Air Vehicle Conference and Competition 2014*, G. C. H. E. De Croon, E. Van Kampen, C. De Wagter, Eds. (Delft University of Technology, Delft, Netherlands, 2014), pp. 280–285.
21. S. Lupashin, A. Schöllig, M. Sherback, R. D'Andrea, in *2010 IEEE International Conference on Robotics and Automation* (IEEE, 2010), pp. 1642–1648.
22. T. L. Hedrick, B. Cheng, X. Deng, *Science* **324**, 252–255 (2009).
23. I. G. Ros, L. C. Bassman, M. A. Badger, A. N. Pierson, A. A. Biewener, *Proc. Natl. Acad. Sci. U.S.A.* **108**, 19990–19995 (2011).
24. K. Ghose, T. K. Horiuchi, P. S. Krishnaprasad, C. F. Moss, *PLOS Biol.* **4**, e108 (2006).

ACKNOWLEDGMENTS

We greatly acknowledge the helpful comments on the manuscript from M. H. Dickinson, M. Kovac, J. L. van Leeuwen, H. Goosen, and B. van Oudheusden. We also thank everyone involved in the earlier stages of the DelFly project, from which we greatly benefited, and especially S. Tijmons for the useful discussions on the robot design and K. M. Kajak for his work on flight dynamics modeling. **Funding:** F.T.M. was supported by a grant from the

Netherlands Organization for Scientific Research, NWO-VENI-863-14-007. **Author contributions:** All authors contributed to the conception of the comparative study and to the analysis and interpretation of the results; M.K. designed and built the robot, performed the robot experiments, and processed the robotic data; F.T.M. provided the fruit fly data; The manuscript was primarily written by M.K., F.T.M., and G.d.C. All authors contributed critically to the drafts and gave final approval for publication. **Competing interests:** M.K. is the inventor on patent application PCT/NL2018/050317 submitted by Delft University of Technology that covers the concept of the flapping wing robot. **Data and materials availability:** All data relevant to the manuscript are deposited as open access data in Dataverse NL: https://hdl.handle.net/10411/ROXE7F.

SUPPLEMENTARY MATERIALS

www.sciencemag.org/content/361/6407/1089/suppl/DC1
Materials and Methods
Supplementary Text
Figs. S1 to S26
Tables S1 to S6
Movies S1 to S10
References (*25*–*29*)

19 January 2018; resubmitted 4 May 2018
Accepted 20 July 2018
10.1126/science.aat0350

Science

A tailless aerial robotic flapper reveals that flies use torque coupling in rapid banked turns

Matej Karásek, Florian T. Muijres, Christophe De Wagter, Bart D. W. Remes and Guido C. H. E. de Croon

Science **361** (6407), 1089-1094.
DOI: 10.1126/science.aat0350

Flying fast and free

Insect flight can be fast and agile, making it hard to study its detailed aerodynamics. Karásek *et al.* designed an untethered, flapping-wing robot with impressive agility that can mimic fruitfly maneuvers (see the Perspective by Ruffier). They studied the robot's motion during rapid banked turns, which revealed that passive motion through the turn generated yaw torque coupling. This correcting yaw rotation propelled the robot toward the escape heading needed for effective turning.

Science, this issue p. 1089; see also p. 1073

Science (print ISSN 0036-8075; online ISSN 1095-9203) is published by the American Association for the Advancement of Science, 1200 New York Avenue NW, Washington, DC 20005. The title *Science* is a registered trademark of AAAS.